# The Structure of a White Dwarf using Runge Kutta Method

C. A. Joynes *

*School of physics and astronomy,*
*University of Southampton,*
*Southampton,*
*SO17 1BJ,*
*United kingdom*

April 26, 2024

**Abstract**

A $4^{th}$ order Runge-Kutta algorithm is used to model the density profile and mass profile of White dwarfs under a relativistic regime acting as a degenerate free Fermi electron gas. Observations of Sirius B, 40 Eri B and Stein 2051 along side data from the SDSS white dwarfs are compared to the model and found consistent with the models predictions. Importantly the Chandrasekhar mass limit is calculated from the model for both C/O/Mg white dwarfs and Fe white dwarfs obtaining values of 1.44 $\pm 7.4^{-4}$ $M_{\odot}$ and 1.246 $\pm 7.4^{-4}$ $M_{\odot}$ respectively. C/O/Mg white dwarfs all have the same Ye value so under are model they can all be considered the same. the Non-Relativistic and Ultra-Relativistic regimes are also tested to verify that a white dwarfs structure is relativistic and best modelled in that regime.

*Electronic address: cj1g21@soton.ac.uk; Corresponding author

# 1 Introduction

Every star will meet one of three ends as it approaches the limits of its evolution. If the star is massive enough, the exhaustion of its fusion fuel will trigger the formation of a Blackhole. Intermediately massive stars will not form a Blackhole but instead a Neutron star, whilst low-mass stars will turn into White dwarfs. According to our current understanding, the primary parameter that determines the final fate of a star is its mass at birth. All stars below a critical mass, believed to be between 6 – 8 solar masses ($M_\odot$) will become a white dwarf, including stars such as our sun. In fact, upwards of 90% [Main1],of all stars will end their evolution as white dwarfs. It is therefore important for astrophysics and the likes, to study these white dwarfs as they are rich forensic laboratories which can provide links between the past and future evolution of the milky way galaxy. The structure of a white dwarf contains the final history of later stages of a stars evolution, as well as being our testing grounds for matter undergoing extreme physical processes near the end of a stars life. Current complex models also consider variables such as rotation, magnetic fields, and atmospheric conditions, however this paper will consider a more basic Fermi degenerate gas model with the aim to come to the same conclusion.

After a main sequence star uses up all their nuclear fuels via the fusion process in which H and He are converted into C and Si and in some cases up to Fe, they cannot support their gravitational inward force and begin to collapse. They will expand up to 100 times their radius and shed their outer layers creating planetary nebulae and leaving behind their cores. The remaining core is what we refer to as a White Dwarf with an average mass of 0.6 $M_\odot$. White Dwarfs have no outward radiation pressure due to the loss of fusion, so the star collapses to radii on scales of the size of the earth. Without a balancing force the white dwarf would collapse entirely however, with ninety-nine percent of the white dwarfs mass contained in the electron degenerate core[Main2] and with the atoms sufficiently close in the material their most weakly bonded electron is free to move around and can be considered to behave as a gas. Almost all electrons will occupy the lowest energy state and any states with the same energy are considered degenerate hence this is known as degenerate electron gas[Main3]. Under conditions of extreme pressure, such as those in the core of a white dwarf, these electrons are forced to occupy spaces much closer to the nuclei than in regular materials. Although, due to Fermi's Exclusion Principal electrons cannot occupy the same quantum state and repel each other to prevent this. In such a material such as a white dwarfs core, it can be shown that the repulsive force is strong enough to support the white dwarf and stop collapse from gravity.

There is however a limit to this repulsive force, known as the Chandrasekhar mass limit. first shown by Chandrasekhar in the 1930's, when an electron degenerate gas is allowed to act realistically, there is a mass limit, $M_Ch \cong 1.459 * (2Ye)^2 M_\odot$[Main4] . With more and more mass added to a star the gravitational force increases and with the repulsive force of electron degeneracy pressure staying relatively equal there is a given amount of mass at which point the degeneracy pressure can no longer support the star anymore and it shall collapse. If a white dwarf is in a binary system with another star, it can gradually accumulate material on the White dwarfs surface. If the accumulated mass surpasses the Chandrasekhar mass limit then we get a type 1a-supernova which is by far the brightest standard candle[Main5]. These Binary systems can also cause material such as Fe and other metals from the companion to accumulate into the White dwarf core. Some proposals suggest that a massive star can gets all its outer layers entirely stripped away revealing just the iron core to produce a Fe White Dwarf. However its estimated that only about $32 \pm 8\%$[Main6] of all white dwarfs are actually in a binary system. Meaning that for most, a White Dwarfs core composition depends on its environment at birth and how the star evolved before becoming a white dwarf. In this paper

we will just focus on carbon and iron core White dwarfs. Where most commonly a White Dwarf will have a carbon (C), Oxygen (O), or a magnesium (Mg) core, for our purposes we can actually considered these all as C core White dwarfs as they all have the same number of electrons per nucleon. The most massive White Dwarfs can reach Iron (Fe) cores. Studying these two different cores allows us to see how the average white dwarf structure compares to the upper scale of a white dwarf with an Fe core. All white dwarfs will have a thin H layer/ envelope which was not burned off when it was still an active star. This hydrogen is left at the surface because the White Dwarf has such a huge surface gravity that all heavier elements settle at deeper layers[Main4] causing the White Dwarf to have elemental layers in its structure.

# 2 Method

Our method is broken into two main steps, the primary is to create two differential equations involving the mass, density and radius of a white dwarf which can be fed into an algorithm and solved numerically. The second is to be able to correctly understand, implement and use the Runge-Kutta algorithm which is used to integrate the previously derived differential equations and plot a model for white dwarfs, given starting parameters and boundary conditions. Our model is under an assumption that the star is spherically symmetric, in hydrostatic equilibrium, non-rotating and acting as a relativistic degenerate Fermi Gas and will be compared with real data from Sirius B, 40 Eri B and Stein 2051 to verify mass and density readings.

## 2.1 manipulating differential equations

White Dwarfs are complex structures and as such have intrinsic properties that change throughout the structure itself, therefore must be described with differential equations rather than linear equations. The stars properties will vary most with its mass and thus it is important to understand how mass changes within a white Dwarf. The mass of a shell with thickness dr is given as,

$$\boxed{\frac{dm(r)}{dr} = 4\pi r^2 \rho} \tag{1}$$

where $\rho$ is the density at a radii r. This is one of our first order differential equation and is debatably the more important one as it will describe the mass profile of our white dwarfs. For our second equation we shall start by balancing the inward Gravitational Force with the outward Pressure of the star,

$$F = \frac{Gm(r)}{r^2} = \frac{dP}{d\rho}\frac{d\rho}{dr} \tag{2}$$

where G is the gravitational constant, and P is the degeneracy Pressure. Here we have implemented the chain rule on the pressure equation and we can see that it depends on a second differential equation known as the equation of state, which can be shown to act as a relativistic free Fermi gas (details in appendix 1) and takes the form,

$$\frac{dP}{d\rho} = Y_e \frac{m_e c^2}{m_p} \gamma(\frac{\rho}{\rho_0}) \tag{3}$$

where Ye is the electrons per nucleon, $m_e$ is the electron mass, $m_p$ is the proton mass and c is the speed of light. Notice in this equation we have $\rho_0 = m_p(m_e)^3 c^3 / 3\pi^2 \hbar^3 Y_e$ which is our average density of white dwarfs. with a gamma function of,

$$\gamma(y) = \frac{y^{2/3}}{3(1+y^{2/3})^{1/2}} \tag{4}$$

if we finally substitute equation (3) into (2) and rearrange for density,

$$\frac{d\rho}{dr} = \frac{m_p}{Y_e m_e c^2 \gamma(\frac{\rho}{\rho_0})} \frac{Gm\rho}{r^2} \tag{5}$$

this gives our other first order differential equation this time for density profiles. Within this we have a lot of constants which can be simplified into a single constant 'C' in Solar units,

$$C = \frac{Gm_p}{Y_e m_e c^2} \approx 0.00387/Ye \tag{6}$$

to finally give

$$\boxed{\frac{d\rho}{dr} = -C \frac{m\rho}{r^2 \gamma(\frac{\rho}{\rho_0})}} \tag{7}$$

the boxed equations (1) and (7) will be fed into our Runge-Kutta algorithm to determine the structure of White dwarfs.

Astronomical units are massive, with values of $10^{30} kg$ this combined with small constants such as $G = 6.67 * 10^{-11} m^3 kg^{-1} s^{-1}$ causes the computational efforts of the computer to be stretched and we would introduce truncation and rounding errors by combining small values with large values in our equations as well as the introductions of recursion errors with our Runge-Kutta algorithm. The method we chose to get around this is to convert all values into astronomical values immediately. This will keep the range of our values within a small magnitude scale which means we wont have massive values combined with microscopic values in our calculations. This helps prevent recursion and rounding errors within our numerical calculation.

### 2.2 Runge-Kutta Method for calculating first order differential equations

As mentioned the second part of our method details how we used a Runge-Kutta algorithm to solve equations (1) and (7). For this problem a $4^{th}$ order Runge-Kutta algorithm should be sufficient at giving good accuracy with out wasting computational time. Since the $4^{th}$ order Runge-Kutta method is a fourth-order method it means that the local truncation error will be on the order of $O(h^5)$ whilst the total accumulated error is order $O(h^4)$. For our model we will use an error of $7.4 * 10^{-4}$[Main7]. To begin both differential equations will depend on each other, as the radius of the white dwarf is integrated over, therefore both equations should be solved simultaneously. To do this both equations will be written into the same function which is solved by the Runge-Kutta algorithm. Secondly as we do not know the final radius of the White dwarfs prior we cannot tell the algorithm to stop at some distance R, instead we shall choose a negligibly small value ($10^{-7}$) for the density. At such a value the density being integrated over is 0.00001% of the core density and we can confidently say that the white dwarf's surface has been reached by this point by approximating the density as zero here and hence we can stop integrating. The boundary conditions of our equations are very important as they will determine much of our model. At 0 radius there should be no mass and hence zero density as well but note that equation (7) is inversely proportional to radius and thus our numerical technique cannot start at a radius of 0, instead let us start our computation at a very small non-zero value; $10^{-10}$ was chosen for our model. Similarly our density can not start at 0 either because of the gamma function in the denominator. This resulted in our final boundary conditions of $r = 10^{-10} R_\odot$, $m = 0\ M_\odot$. for our density profile we needed a single core density and chose $\rho = \rho_0$.

Under the same assumptions and constraints our mass profile can be created by running our Runge-Kutta algorithm many times, the boundary conditions will be kept the same as before apart from this time we set $\rho = \rho_c$, where $\rho_c$ is a set of densities which range from low to high values. The core densities can then be looped over and when each calculation terminates at the white dwarf surface, the final radius is recorded and its respectively mass is appended to a separate list (details in appendix 2). With a new set of radii and mass for a range of densities the mass profile of a white dwarf can be plotted and the relative observed data can be overlaid atop of it to confirm the model. Once all parameters and boundary conditions are set we can cycle through both Ye values for carbon and iron respectively and obtain the 2 lines for each plot which we can later compare in our results section.

# 3 Results and discussion

## 3.1 relativistic model

Our aim in our results is to create a model for white dwarfs density and mass profiles under a relativistic regime in which the cores are described by a degenerate Fermi Gas of electrons. White dwarfs are faint objects which are difficult to see and harder to measure, because of this there is very limited data on them with only 3 observed white dwarfs from which we recall data from; Sirius B, 40 Eri B and Stein 2051. These three white dwarfs however have been well documented enough by telescope observations and have reliable data on their mass and radius for which we can compare our models too.

To begin our results, we first dive into our relativistic density profile plot in figure 1. This plot shows both the carbon and iron core white dwarf's density change as a function of radius.

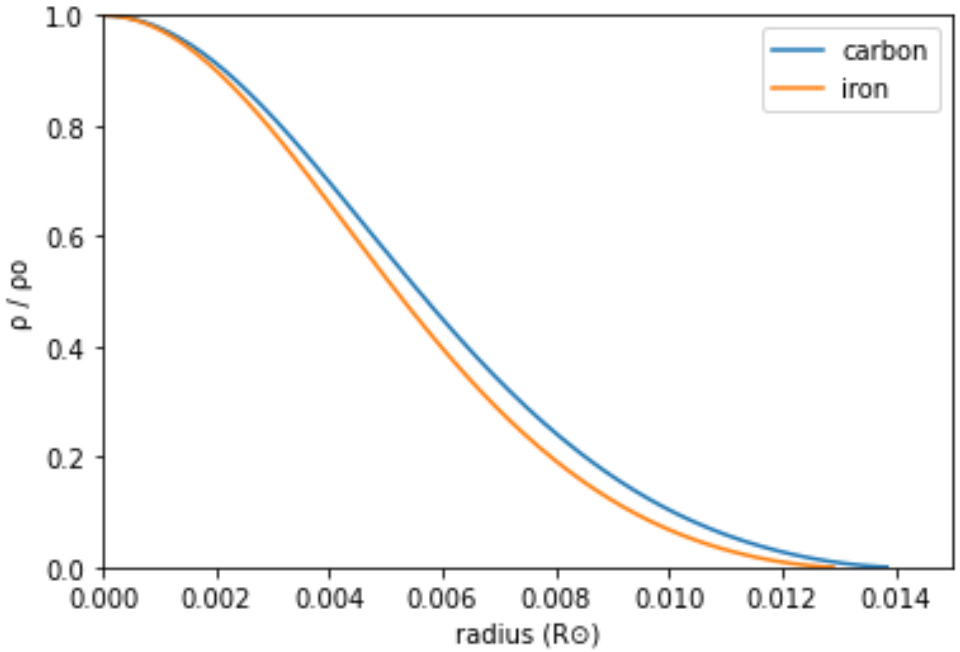


Figure 1: density profile for C and Fe core white dwarfs under a relativistic regime using a degenerate free electron Fermi gas model.

Notice in figure 1 we use the dimensionless quantity $\frac{\rho}{\rho_0}$ on the y axis, this shows us how the density of the white dwarf changes with radius as a value of the core density $\rho_0$. We chose this as it allows for easier reading of how the density varies as we move out from the core. Importantly we can see how the composition of the core changes the density profile with the iron core dropping off in density quicker than the carbon core. From the plot we can infer that this means that iron core White dwarfs have more of their mass confined within smaller radii than that of carbon core White dwarfs. In main sequence stars denser cores usually means higher temperature but white dwarfs are isothermal meaning almost all the mass of the white dwarf will be the same temperature as well as their temperature dependence being degenerate means that their physical properties do not depend on temperature.

Under the assumptions set within our method section, we know that as our density reaches zero we can assume that we have reached the white dwarfs surface and hence the corresponding value for radius must be the maximum size of the white dwarf for core density $\rho_0$. Our model predicts a maximum size of 0.01386 $\pm 7.4^{-4}$ $R_\odot$ for Carbon cores and 0.01286 $\pm 7.4^{-4}$ $R_\odot$ for Iron cores. the radius of the earth is 0.009168 $R_\odot$ meaning white dwarfs are of the same scale as the earth. From our plot we can see that the middle section of the plot is almost linear meaning that the structure doesn't change much through the main body of the white dwarf, however at the centre and the surface, the plot appears to have a power law resemblance indicating a rapidly changing structure in these regions.

Next, we want to find the mass profile of a white dwarf, we can do this using the technique in the methods section and detailed in appendix 2. We then fitted the chosen stars of known mass and radii onto our model and found that they agreed with our model with Sirius B aligning with carbon cores best whilst both 40 Eri B and Stein 2051 seem to fit iron cores better.

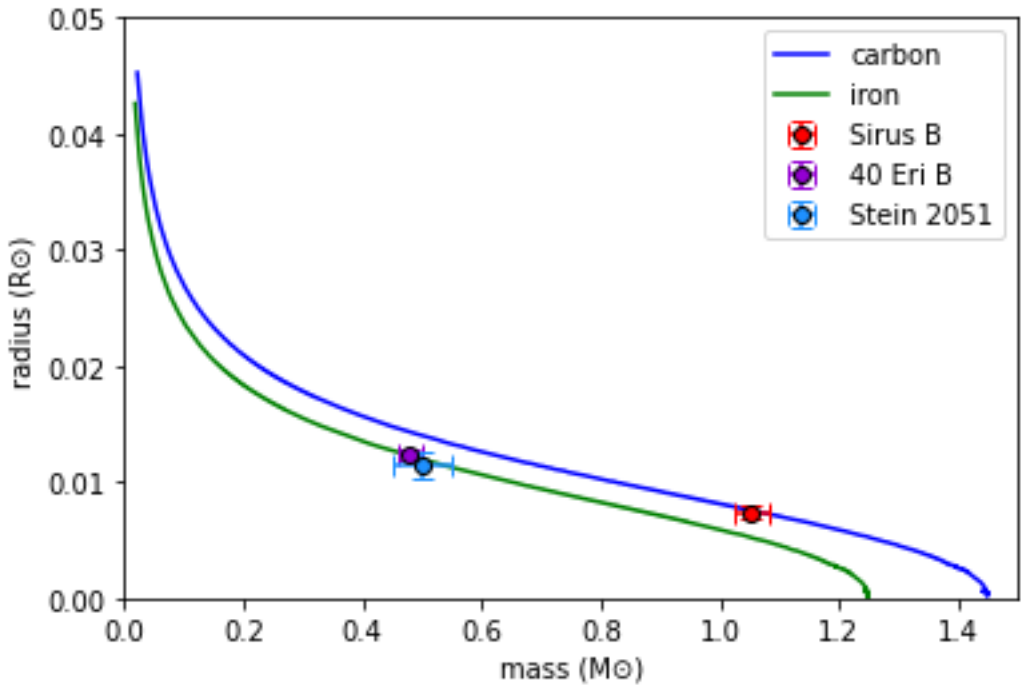


Figure 2: mass profile for C and Fe core white dwarfs. the well documented observational data of know sources are plotted on top of the model. observations have errors which agree with our model.

As the mass of a white dwarf increases its radius decreases, this may at first seem wrong as normally stars radii increase with their mass as the additional gravitational force causes more fusion within the core which will increase the outward pressure allowing the star to grow in size, however with a white dwarf, the increase in gravitational force cannot be counteracted by fusion as white dwarf stars are considered 'dead' and the outward electron degeneracy pressure stays relatively equal hence the star size reduces with increased mass. This is until a given mass is reached and the star collapses. This is known as the Chandrasekhar mass limit and is usually recalled as 1.44 $M_{\odot}$[Main8]. This is the limit for C/O/Mg white dwarfs and so we can return this limit from our carbon mass profile. If a White Dwarf gains mass greater than $M_{Ch}$, the collapse will trigger a type 1a supernova. If the stars mass was always greater than the Chandrasekhar mass limit then the star would have become either a Blackhole or a Neutron star at the end of its evolution.

Similar to the density profile where we could calculate the white dwarfs maximum radius, from the mass profile we can determine the white dwarfs maximum mass. The maximum mass is important because this defines the Chandrasekhar mass limit for white Dwarfs. Our model predicts that Carbon core white dwarfs will have a maximum mass of 1.44 $\pm 7.4^{-4}$ $M_{\odot}$ which agrees with studies. As suspected the Chandrasekhar mass limit should be smaller for iron given its higher density, and our model agrees with a predicted maximum mass of 1.246 $\pm 7.4^{-4}$ $M_{\odot}$, which differs by only 1.2% to other theoretical predictions of the iron mass limit with similar values of 1.258 $M_{\odot}$[Main4].

Given that the mass of the White dwarf is the only dependant variables for its properties in our model, it was plotted on the x-axis. Looking at the plot, we can show that the low-mass section of the model is best described as an ideal gas pressure dominated with a high-power law the steep drop. Around 0.2 $M_{\odot}$ the plot appears to even out and we enter the relativistic degenerate gas regime. This part of the graph has a gradient slope of $-\frac{1}{3}$ with an equation of pressure, $P \sim \rho^{5/3}$, and polytrope index of $\frac{3}{2}$. Our experimental data points are found within this relativistic regime which is expected as their average mass is 0.6 $M_{\odot}$, with most White dwarf masses lying in the range of 0.5-0.8 $M_{\odot}$. Following the plot into the high-mass part we can see a dramatic cut off as it enters the ultra-relativistic degenerate gas regime, where the radius decreases to zero at the Chandrasekhar mass limit.

### 3.2 SDSS data set

The aim of this report is to model the structure of a White dwarf, so to test our model further and verify that the model is correct we went to the Sloan digital sky survey which looked at thousands of stars including white dwarfs. Using observable parameters such as luminosity and temperature[Main9], the SDSS data set calculated theoretical masses and radii for many white dwarfs, this set of theoretical data is what we shall use to help confirm our model by comparison. 15 different white dwarf's data points were plotted on top of our model alongside the previously labelled stars. The SDSS data points all have errors correlated with their mass and radius which allows us to confidently confirm that our model agrees with the data set.

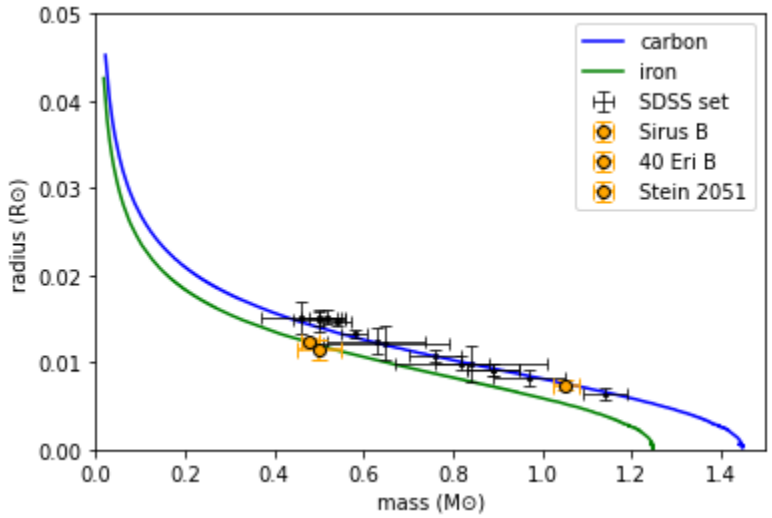


Figure 3: Mass profile plot with an additional 15 data points from the Sloan Digital Sky Survey (SDSS) [Main10] to further verify the model. previously mentioned observational data in orange

As well as the errors correlated with the SDSS data set we can check quantitatively how well the theoretical data fits our model. Given the model has polynomial characteristics which we discussed earlier, we've chose to use a polynomial fit. the degree of order chosen is a hyperparamater and should be chosen wisely. using to high of a degree polynomial will over-fit the data, whilst using to low of a degree polynomial will under-fit the data[Main11]. Considering we are only interested in the region where the SDSS data lies we can fit specifically for there. From Observation we know that the degree should be between 1-3, and after testing all the options, a polynomial degree of order 3 is best to get a good fit for our data. comparing the model with the fitted line we get an error of $6.99 * 10^{-8}$ and a deviation of $2.64 * 10^{-4}$ for our model. taking into account our models magnitude this means that the SDSS data has a derivation from our model of $\sim 0.025\%$ which is very small and quantitatively confirms that our model is a good fit for the data.

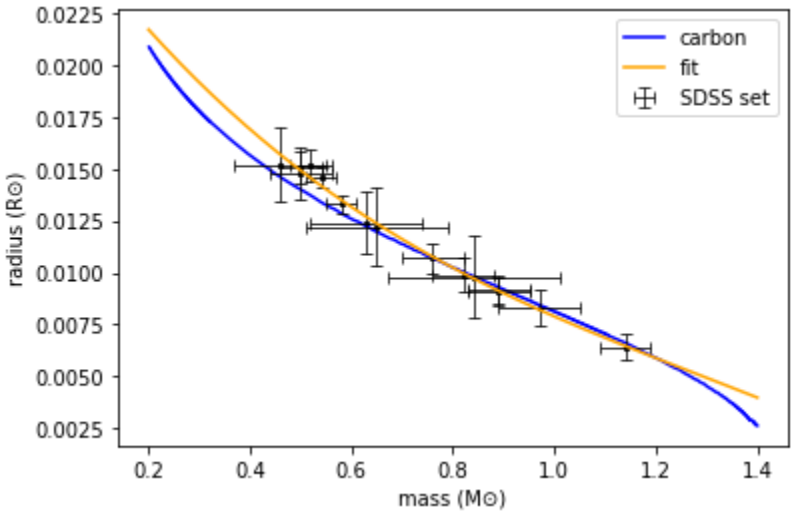


Figure 4: C white dwarf mass profile with SDSS data, in limits of 0.2-1.4$M_{\odot}$ on the plot, orange line is fitted with polynomial fit

### 3.3 Non-relativistic and Ultra-relativistic regimes

Although we have shown that white dwarfs follow a relativistic regime with electrons moving at relative speed of light speeds inside the core of a white Dwarf, its good to show how this differs to a Non-relativistic model and what happens at the Ultra-relativistic limit as well.

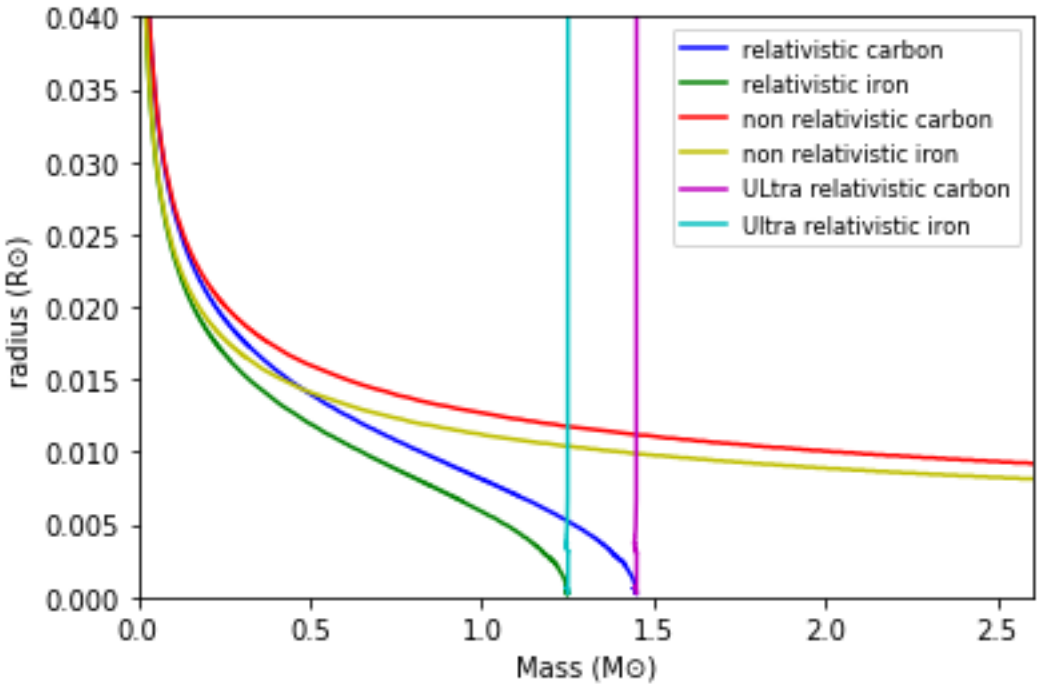


Figure 5: the degenerate free Fermi electron gas model for Non-relativistic and Ultra-relativistic regimes plotted along side the relativistic regime model.

To start we can see that the Ultra-relativistic model, where the electron speed is modelled as the speed of light, is a vertical line at the two Chandrasekhar mass limit for carbon and iron respectively. This tells us that as the mass of the white dwarf increases to its maximum mass, it causes the electrons inside the core of the white dwarf to accelerate and begin to move at speeds equivalent to the speed of light. Obviously electrons have a mass and so cannot actually move at c, which is another reason the model breaks down at masses greater than the Chandrasekhar mass limit.

Now looking at the Non-relativistic model, at small masses the models are similar, which is expected because at small masses the electrons are barley moving at relativistic speeds. As the mass is increased the two models begin to diverge for both the C and Fe core white dwarfs. The diversion begins at about 0.2 $M_{\odot}$ and the gap only increases until the relativistic model hits the Chandrasekhar mass limit where it stops. Whereas the Non-relativistic model continues on past the Chandrasekhar mass limit and in fact will continue on forever as its asymptotic meaning the electrons in the core could gain infinite energy which is incorrect and hence the Non-relativistic model is wrong.

### 3.4 additional research and limitations

Our model is under the assumption that white dwarfs are stationary non-magnetic objects. In reality the majority of white Dwarfs are rapidly rotating objects with large magnetic fields.

Research into the affect of rotation on the mass function of a white dwarf shows that rapidly rotating white dwarfs appear to have larger masses at small radii than stationary

white dwarfs, whilst at larger radii both static and rotating white dwarfs tend to the same mass. In a study about rotation and temperature and their effect on the mass function of a white dwarf, it was shown that both parameters resulted in an increased mass.

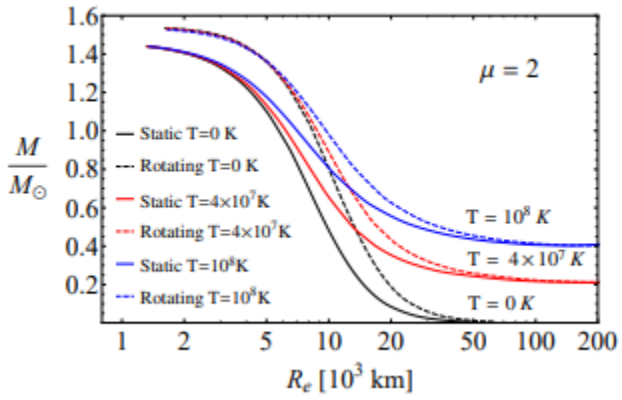


Figure 6: Mass profile for C white dwarfs. Solid curves show static and dashed curves show rotating white dwarfs for temperatures T = $[0, 4^7, 10^8]$ K [Main12].

Other models investigate the affect of magnetic fields which arise from the rapidly moving electrons in the core. Current study shows that high magnetic field white dwarfs having a larger mean mass ($\sim 0.93 M_\odot$)[Main13] compare to low magnetic field white dwarfs, which have a mean mass of $\sim 0.58 M_\odot$. From this research the mass function would have a 160% increase on our current model which doesn't include magnetic fields. This is a significant change on the mass function and therefore sets a limitation on our model. On the other hand the increase in mass could be an explanation for large magnetic fields rather than the other way around. The study found that isolated white dwarfs were divided into two main categories: ones that have arisen from a single star evolution and ones that have passed through one or two phases of binary evolution. The former usually results in C/O/Mg white dwarfs. Whilst the latter group contains a larger range of different white dwarfs. Since binary-evolution tends to create more massive white dwarfs with more free electrons and are more likely to have iron core, they tend to have increased magnetic fields. Which may explain why white dwarfs with high magnetic fields have a higher average mass.

Other Observations of type 1a supernova have indicated that white dwarfs with very large magnetic fields may be able to exceed the Chandrasekhar mass limit. Our model is based of the balance of gravitational pressure with electron degeneracy pressure, however with large magnetic fields white dwarfs may also experience a second outward pressure due to the magnetic field and could therefore support more mass than our model predicts. It can be shown that with the addition of large magnetic fields that the Chandrasekhar mass limit could be as high as 2.58 $M_\odot$[Main14] which would disagree with our current model and is another limitation for us.

White dwarfs have been observed to go above the Chandrasekhar mass limit before but only in specific cases. The first is when a white dwarf is in a binary system with another stellar object such as a red giant. Usually involving the growth of a carbon-oxygen white dwarf which will accrete matter from its stellar partner until it reaches the Chandrasekhar mass limit where it will trigger a type 1a supernova[Main15]. Alternatively the helium envelope of these white dwarfs could suddenly undergo fusion which would rapidly compress the core with a shock wave from the ignition and the star could exceed the limit this way. The Final scenario is a binary system containing two white dwarfs. A galactic event could trigger gravitational waves which would lead to the coalescence of the close pairs of compact objects[Main16]. The less

massive of the two white dwarfs would then be torn apart by tidal forces and absorbed by the more massive of the pair. The latter would exceed the Chandrasekhar mass limit and collapse before thermonuclear runaway.

# 4 conclusion

We used a fourth-order Runge-Kutta algorithm by fixing boundary conditions such as mass, density and radius, to create a degenerate free Fermi gas model for white dwarfs in a relativistic regime. Once we had our model we could create a density profile for a single white dwarf of core density $\rho_0$ and a mass profile for all white dwarfs. With this we could then use our 3 well documented observed white dwarfs and the theoretical data of 15 additional white dwarfs from the Sloan digital sky survey data release to compare to our model and confirm the success of it. The SDSS data has an error of $6.99 * 10^{-8}$ telling us that the model fitted the data very successfully and could be used to fit other white dwarfs. With the model confirmed to be solid we could then obtain the Chandrasekhar mass limit for both carbon and iron core White Dwarfs, getting $1.44 \pm 7.4^{-4} M_{\odot}$ and $1.246 \pm 7.4^{-4}$ $M_{\odot}$ respectively, which would agree with previously documented values. We could also confirm that the White dwarfs must be in the relativistic regime as both the non-relativistic and ultra-relativistic regime were tested and disproven.

## Appendix 1: Relativistic Model

in this appendix we will show the derivation of the model for a free Fermi gas in a relativistic regime[Main17] and aim to show:

$$\frac{dP}{d\rho} = Y_e \frac{m_e c^2}{m_p} \gamma(\frac{\rho}{\rho_0}) \tag{8}$$

where,

$$\gamma(y) = \frac{y^{2/3}}{3(1+y^{2/3})^{1/2}} \tag{9}$$

The equation for Pressure of a gas is,

$$P = \frac{1}{3} n < pv >= \frac{1}{3} \int_0^\infty n(p) pv dp, \tag{10}$$

here we have written number density n as a function of momentum, p, giving,

$$n(p) = \left\{ \begin{array}{ll} \frac{8\pi}{h^3} p^2 & \text{if } p < p_F \\ 0 & \text{if } p > p_F \end{array} \right\}$$

The Fermi momentum $p_F$ is given by,

$$n = \frac{8\pi}{h^3} \int_0^{p_F} p^2 dp = \frac{8\pi}{3h^3} p_F^3 \rightarrow p_F = \left( \frac{3h^3}{8\pi} \frac{\rho}{\mu m_u} \right)^{1/3} \tag{11}$$

Now that we have the Fermi momentum we should next tackle the fact that we are in a relativistic regime. The energy can be recast in terms of the relativistic gamma function (different to $\gamma(y)$),

$$(m_e c^2)^2 + (pc)^2 = \gamma^2 (m_e c^2)^2 \tag{12}$$

where gamma is,

$$\gamma = \frac{1}{\sqrt{1 - (\frac{v}{c})^2}} \tag{13}$$

we can then use equations (12) and (13) to rearrange for the velocity,

$$v(p) = c \left[ 1 - \frac{1}{1 + (\frac{p}{m_e c^2})^2} \right] \tag{14}$$

and then substituting (14) into (10) ate the Fermi momentum limit returns,

$$P = \frac{1}{3} \int_0^{p_F} \frac{8\pi}{h^3} p^2 p v(p_F) dp, \tag{15}$$

Recalling the result we are trying to show, we see that our result is a differential that depends on density so lets use the chain rule, $\frac{dP}{d\rho} = \frac{dP}{dp} \frac{dp}{d\rho}$ and then this yields,

$$\frac{dP}{d\rho} = \frac{8\pi}{3h^3} p_F^3 v(p_F) \frac{dp}{d\rho}|_{p_F}, \tag{16}$$

from here we can substitute in the Fermi momentum from (11) and rearrange to get,

$$\frac{dP}{d\rho} = \frac{1}{3} \frac{\rho^{1/3}}{\mu m_u} c \left[ \frac{1}{1 + (\frac{m_e c^2}{p_F})^2} \right]^{1/2} \left[ \frac{3h^3}{8\pi} \frac{1}{\mu m_u} \right]^{1/3} \tag{17}$$

using the relation $p_F \sim p^{1/3}$, and hence $\frac{p_F}{m_e c^2} \sim \frac{\rho}{\rho_0}^{1/3}$ we finally get the result as required,

$$\frac{dP}{d\rho} = Y_e \frac{m_e c^2}{m_p} \frac{y^{2/3}}{3(1+y^{2/3})^{1/2}} \tag{18}$$

## Appendix 2: Mass Profile

figure 2 and the proceeding figure for the mass-radius relation are the most important relations in this report and therefore we have decided to include more details in this appendix about how we got the mass profile plot. As mentioned in the method (section 2.2) we have an array of core densities $\rho_c$ ranging from $10^{-4}$ to $10^{12}$ $M_\odot/{R_\odot}^3$. This array was cycled through and for each density the mass radius relation was plotted. Each line ends when the density of the star reaches our designated cut off value. Then the coordinates of the end point of each line was recorded and appended to a separate list to be plotted later which would give us the final mass profile plot we desire.

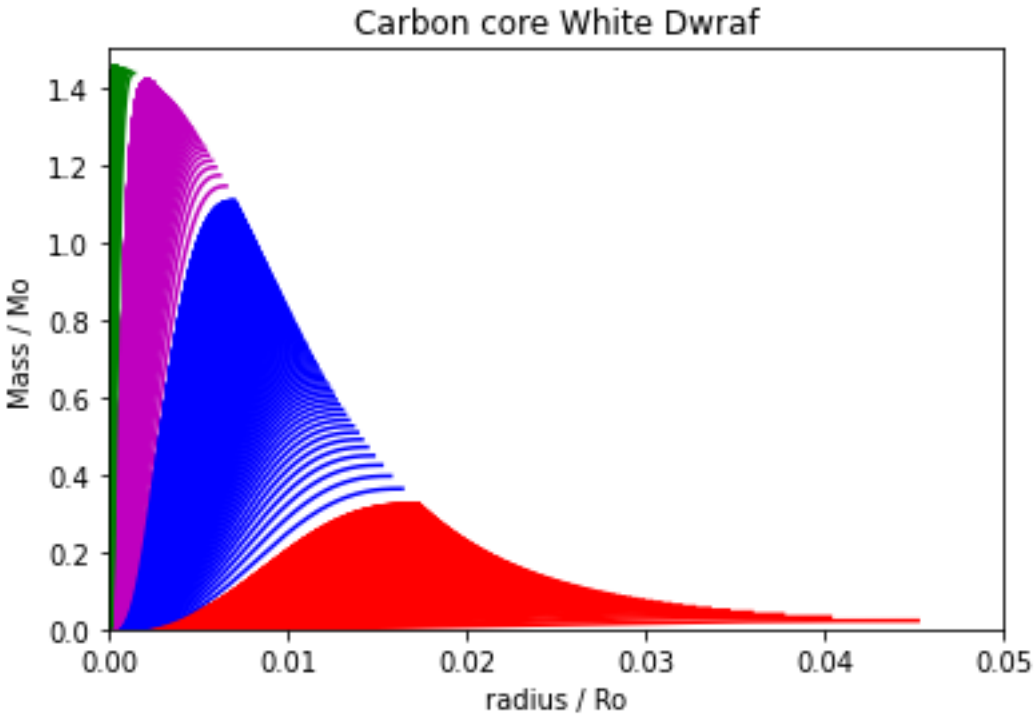


Figure 7

Importantly for our range of core densities, $\rho_c$, we split this into 4 subsets: a low density (red), two medium density sets (blue and magenta) and a high density one (green). This allowed us to loop over each section for a relatively small number of iterations whilst keeping the wanted accuracy high. We adjusted the sizes of each set according to how much a change in core density effects the final mass. For the lowest densities the range can be large as a small change in density here wont change the total enclosed mass much. For medium sets we allowed a small range as the results are most volatile in this section and a small change in core density here will have a large affect on the end mass. The high density region was also kept small as this will define the maximum mass of the white dwarf which is a very important result for us, so we want to keep the range of this set small so the maximum mass can be calculated with high precision

## Appendix 3: Non-Relativistic Model

In our discussion section we used a Non-relativistic regime but never mentioned how we created this profile, so we shall show that in this appendix. In a Non-Relativistic regime the electrons move classically and so have velocity $v(p) = \frac{p}{m_e}$, this results in a pressure equation such as,

$$P = \frac{1}{3}\int_0^\infty n(p)\frac{p^2}{m_e}dp, \tag{19}$$

then following similar procedure as the relativistic case we get,

$$\frac{dP}{d\rho} = Y_e\frac{m_e c^2}{3m_p}\left(\frac{\rho}{\rho_0}\right)^{2/3} \tag{20}$$

Then following the setup laid out in the method (section 2.1) this will give the final equations that can be used in the Runge-Kutta algorithm,

$$\frac{d\rho}{dr} = -C^*\frac{m\rho^{1/3}\rho_0^{2/3}}{r^2} \tag{21}$$

$$C^* = \frac{3Gm_p}{Y_e m_e c^2} \tag{22}$$

note that for all three regimes the mass radius equation remains the same.

## Appendix 4: Ultra-Relativistic Model

Similarly to Non-Relativistic, Ultra-Relativistic was used in section 3.3 and in that section it wasn't explained how we got the result so that will be discussed here. In a Ultra-Relativistic regime the electrons move at the speed of light,$c = \frac{p}{m_e}$, this results in a pressure equation such as,

$$P = \frac{1}{3}\int_0^\infty n(p)cdp, \tag{23}$$

again following similar procedure as the relativistic case we get,

$$\frac{dP}{d\rho} = Y_e\frac{m_e c^2}{3m_p}\left(\frac{\rho}{\rho_0}\right)^{1/3} \tag{24}$$

This then results in a slightly different end result,

$$\frac{d\rho}{dr} = -C^*\frac{m\rho^{2/3}\rho_0^{1/3}}{r^2} \tag{25}$$

$C^*$ is the same as in the Non-relativistic regime and again the mass-radius relation is the same as before.

## Main References


[Main1] Detlev Koester and Ganesar Chanmugam. Physics of white dwarf stars. *Reports on Progress in Physics*, 53(7):837, 1990.

[Main2] JL Provencal. The importance of white dwarf stars as tests of stellar physics and galactic evolution.

[Main3] MA Barstow and K Werner. Structure and evolution of white dwarfs and their interaction with the local interstellar medium. *Astrophysics and Space Science*, 303:3–16, 2006.

[Main4] Onno Rudolf Pols. *Stellar structure and evolution*. Astronomical Institute Utrecht NY, 2011.

[Main5] Dina Prialnik. *An introduction to the theory of stellar structure and evolution*. Cambridge University Press, 2000.

[Main6] JB Holberg. What fraction of white dwarfs are members of binary systems? In *Journal of Physics: Conference Series*, volume 172, page 012022. IOP Publishing, 2009.

[Main7] R Fitzpatrick. Runge-kutta methods.

[Main8] Subrahmanyan Chandrasekhar and Subrahmanyan Chandrasekhar. *An introduction to the study of stellar structure*, volume 2. Courier Corporation, 1957.

[Main9] Souza Oliveira Kepler, Scot James Kleinman, Atsuko Nitta, Detlev Koester, Bárbara Garcia Castanheira, O Giovannini, Alex Fabiano Murillo da Costa, and L Althaus. White dwarf mass distribution in the sdss. *Monthly Notices of the Royal Astronomical Society*, 375(4):1315–1324, 2007.

[Main10] Qi Hu, Chaolun Wu, and X-B Wu. The mass and luminosity functions and the formation rate of da white dwarfs in the sloan digital sky survey. *Astronomy & Astrophysics*, 466(2):627–639, 2007.

[Main11] R Agrawal. Master polynomial regression with easy-to-follow tutorials. *Analytics Vidhya*, 2021.

[Main12] Kuantay Boshkayev, Orlando Luongo, Marco Muccino, and Hernando Quevedo. Static and rotating white dwarf stars at finite temperatures. *International Journal of Mathematics and Physics*, 12(2):61–69, 2021.

[Main13] Lilia Ferrario and DT Wickramasinghe. Magnetic fields and rotation in white dwarfs and neutron stars. *Monthly Notices of the Royal Astronomical Society*, 356(2):615–620, 2005.

[Main14] KS Jayaraman. New mass limit for white dwarfs. *Nature India*, 2013.

[Main15] JW Truran Jr, A Heger, and DH Heinrich. Treatise on geochemistry. 1, 2003.

[Main16] Vasilii V Gvaramadze, Götz Gräfener, Norbert Langer, Olga V Maryeva, Alexei Y Kniazev, Alexander S Moskvitin, and Olga I Spiridonova. A massive white-dwarf merger product before final collapse. *Nature*, 569(7758):684–687, 2019.

[Main17] Onno Rudolf Pols. *Stellar structure and evolution*. Astronomical Institute Utrecht NY, 2011.

# Addendum

C. A. Joynes *

*School of physics and astronomy,*
*University of Southampton,*
*Southampton,*
*SO17 1BJ,*
*United kingdom*

April 26, 2024

## 5 random Numbers

Random numbers are used almost everywhere in Academia, often for very similar reasons. One reason outlined by [Addendum1] is random sampling. Sampling is when you want to study some characteristic about a population, but you cannot research and question every individual in the entire census so you need to sample a smaller volume with characteristics that will reflect the entire populations. However the issue with Random sampling is there is usually lots of bias when choosing whats included in your sample. Random numbers can get around this because we can assign an index to our population and then use a random number generator to generate X amount of people for the sample and depending on the numbers generated is who we would choose for the random sample.

Another way random numbers are used in Academia is to simulate he radioactive alpha decay. This is a process which appears in nature and is based around randomness. Radioactive decay is when an unstable isotope decays into a different element, however the chance of a decay is on a random time scale. [Addendum2] describes a simulation for this decay where we have a number $N_0$ which will represent the total number of nuclei in the isotope. We can then use a RNG to generate $N_0$ random numbers between 0-1. A decay constant $\lambda$ is set depending on the isotope, and if the randomly generated numbers are less than $\lambda$ then they will be 'decayed' and removed. The simulation continues again this time we generate $N_0 - N$ random numbers between 0-1. This simulation works well to describe the half-life of alpha decay.

True randomness is very hard to achieve and many simulations use pseudo-randomness but True randomness can be obtained from processes such as alpha decay or things like electrical noise. Entropy is a measure of randomness, true random number generators use an entropy source and must be unpredictable in principle[Addendum3]. Electrical noise is inevitable and unpredictable which is normally why scientists dislike it as its hard to remove, however in this case, the complete randomness of the electrical noise can be used to create random numbers from true randomness. Of course the reverse can be applied to data and random number can be used to remove noise from data .

*Electronic address: cj1g21@soton.ac.uk; Corresponding author
*Electronic address: cj1g21@soton.ac.uk; Corresponding author

Continuing the discussion about True random number generators there are also such things called pseudo random number generators, most RNG use pseudo-randomness rather than true randomness as its easier to do. [Addendum4] discusses how different random numbers are more secure than others because in the world or encryption the randomness of a number can determine how safe your data is. The largest use for RNG in industry is encryption where data is randomly changed to prevent outside views from being able to read and use your data. Pseudo random numbers are generated using a seed and have to create entropy, some can use seeds such as current time, location or even mouse position but these are all predictable and therefore can be decryptable. True random generators such as alpha decay, atmospheric noise and lasers allows for more secure encryption.

Other areas of industry that use random numbers include the lottery. The lottery has been recorded back to 200BCE and since then has always depended on random number generation to select the winning combination of numbers. Traditional lottery machines often use a when and balls to determine winning numbers, however as laid out in [Addendum5] and previously this is not true randomness but instead is pseudo randomness. Modern lotteries use random number generation to select the winning numbers, these often have millions of possibilities and outcomes but these too are often not true random number generators.

Another huge and growing sector in industry is gaming. Gaming often uses and manipulates random numbers. [Addendum6] discusses how two similar games differ on a game play mechanic as one uses randomness and the other does not. The paper describes 'counter strike: global offensive' and mentions how the spray of bullets from the guns are not random and in fact have a set pattern to them which players can learn and use. It allows players to move their aim according to the pattern. Alternatively in 'Player Unknown Battle Ground' the spray pattern of the gun is based of a random number generator meaning there is no way of players to pre-determine the pattern and cannot move their aim pre-emptively. This small difference between whether a game uses random number generation for a single aspect has a huge difference in the game play, mechanics and feel of the two games.

## 6 random walks

The Stochastic process is based in probability theory where a process of determining a probable location of a point is subject to random motion. Stochastic motion is therefore a clear process in academia of random walks. The stochastic process is one of the most generic processes where a set of random variables is indexed against another set of variables[Addendum7]. It has strong links to random numbers and processes discussed in section 5 such as alpha decay.

The article [Addendum8] talks about another process in Academia where we optimize random walks: diffusion. Diffusion is the process by which molecules move from areas of high concentration to low concentration. [Addendum8] describes how this description is slightly flawed because as the diffusing substance moves around the environment (given its not in a vacuum) it will collide with air and other particles causing a type of Brownian motion. It is this Brownian motion of the diffusing substance which we can model using random walks and in turn it means we can model the diffusing gas.

Mainly used in engineering but other fields as well including computing and mathematics, random walks have been used to construct algorithms to gain information on networks called link-prediction. Inside the world of link prediction there are many different methods and algorithms tailored to specific needs and desires of the network. One example of those algorithms is node2vec which uses biased random walks to realise embedding nodes into low-dimensional space which can then be used for link prediction[Addendum9]. As mentioned node2vec is a biased random walk meaning it follows a random path but it considers the previous nodes its visited as well as the network in total. Applications of node2vec, and by proxy random

walks, differ from predicting gene association with Parkinson's disease to movie recommendations. Link prediction is very important because it allows you to find missing links in static networks. But in a dynamic network, which most networks these days are, link prediction is used to predict the likelihood of future links on the network.

This link prediction model is also found applicable in the industry world. Google page rank algorithm is based of clustering algorithms with nearly-linear time and space complexity. clusters are sub-graphs that are highly intra-connected and have a low -inter-connectivity. [Addendum10] Details how the algorithm employs the inherent cluster exploratory property of random walks to reveal the cluster of a given graph. Specifically google rank algorithm starts from a vertex with man limited length random walks, it then wanders the network and records the number of visits at each new vertex as well as the number of connected vertices to the current one. The algorithm then sorts the vertices according to the number of visits and connections.

As we try to put COVID behind us its important to know that random walks can help us to predict, study and defend against real pandemics and diseases such as the infamous COVID-19. Such spreads can be successfully modelled using random walks, [Addendum11] discusses this modelling of epidemics. The articles says that such models rely on the fact that they can be modelled as a random walk, where the systems transitions from state to state within a given time and a set probability that depends on the current node of the system. epidemic and disease spread can be simplified to be modelled this way. The article also discusses limitations of this model, stating that many times it over predicts time scales of events because it does not consider the simultaneous presence of infected people well. It does however give a good understanding of how the infection can spread though a population and allows us to investigate possible control techniques earlier than ever before which can save lives.

Staying inside the medical world, random walks have great implications in treatment management and diagnoses. certain drugs are critical to the recovery and development of patients however to little can be ineffective and to much can cause more harm, so getting the correct dosage is a very important aspect of the medical world. Following this, in many cases the original dose level; prescribed to patients is far below the anticipated recommended does for safety reasons. This is beginning to change as in this study [Addendum12] researchers are using random walks alongside medical ethical consideration as well as patient response to further understand the way in which these substances are absorbed into the body. The study demonstrates the use of a random walk algorithm which is applied to a lattice of dose levels to calculate what dosage should be tested for allowing patients to receive improved care.

## 7 Monte Carlo Simulation

As detailed at the end of section 6 random walks can be used in medicine to allow for better dose prediction, similarly people are using Monte Carlo simulations in modern radiotherapy treatment planning. Electron of high energy only really scatter via 2 procedures, Compton scattering ad pair production. The probability of each scattering type per cm can be considered constant. Radiotherapists want to determine if and how much radiation will reach the target zone of the patient a distance x cm into the body. A way of doing this is to create a Monte Carlo simulation where many electrons entering a given material, such as the brain, are simulated and tested to see how far the electrons make it before scattering and of what type [Addendum13]. The simulation can be run many times to allow the radiotherapist to determine the average location and depth. This technique helps determine the dosage and creates better planning for the treatment.

Elsewhere is industry, Monte Carlo has been used to account for many different outcomes. This is an important skill as the future is inherently unpredictable and has a degree of uncertainty. Within finance, Monte Carlo is used to generate lots of random portfolios of stocks and then for each portfolio it calculates the estimated risk and return characteristics. That information is then used to choose the best portfolio for a given interested objective.[Addendum14] also talks about how investors can use Monte Carlo simulations to model the likelihood of different outcomes especially when there is uncertainty surrounding the inputs. Particularly good for taking on portfolios with an inherent amount of risk.

Other areas that use this technique include weather forecasting. Weather is a continuous and never-ending process, with new data constantly being generated. Weather has been recorded since humans were able to write creating a huge data base of information to use. [Addendum15] explains how variables such as temperature, rainfall, pressure and more can all be used to model and predict future outcomes. Probability distributions can then be assigned to the variables based of the historical data, expert opinion and uncertainty probability to model the data. the article then describes how a Monte Carlo simulation can be used to randomly simulate different weather events and determine the probabilistic one and forecast it.

The study of our environment is also done academically. Atmospheric dust can have many negative side effects to our world and its ecosystems, such as soil erosion, land degradation, vegetation loss and more. It can also impact the health of people in areas with high atmospheric dust. Therefore it is an important topic to understand, research and try to improve. In the report [Addendum16] a Monte Carlo simulation was applied to map the source contributions of atmospheric dust samples collected from Iran. The study also compared another simulation technique for the investigation, finding both methods had recovered a mean-absolute-fit and goodness-of-fit of ¿80% with the Monte Carlo simulation scoring slightly better. The case study is a direct example of how Monte Carlo simulations is a tool that can be used to better the understanding of our world and help improve the lives of people today.

In other areas of academia,people are using high-precision Monte Carlo to model galaxy distribution. Within the paper [Addendum17] it details how fast Monte Carlo can be used to determine galaxy positioning for non-Gaussian fields. this is done by creating a random matter distribution that is not Gaussian as well as a density field to simulate space expansion to then estimate positions of galaxies. Along side this is the NASA report [Addendum18] which talks more in depth about how astronomers use Monte Carlo to simulate the orientation of the galaxies within their clusters. This relates to the first report but zoomed in more to scales of individual clusters rather than larger scales of our universe. These uses of Monte Carlo simulations are more computationally heavy than other areas of expertise that are using Monte Carlo and hence often find that they are using different software and specific programming languages which can handle these intense simulations.

Monte Carlo in engineering is widespread for the express purpose of quantitative probabilistic and sensitivity analysis within process design. This gets over deterministic methods downfalls and therefore reduced errors which will lead to less instability in your design. For example, this Monte Carlo sensitivity analysis is being used in microelectronics engineering to correctly analyse and make accurate predictions about correlated and uncorrelated variations in analog and digital integrated circuits [Addendum19]. Monte Carlo in sensitivity analysis is far more realistic at interpreting uncertainty within a risk analysis variable.

## Addendum References


[Addendum1] Shagofah Noor, Omid Tajik, and Jawad Golzar. Simple random sampling. 1:78–82, 12 2022.

[Addendum2] Sahajpreet Singh. Monte carlo simulation of radioactive decay. 5:86–90, 09 2020.

[Addendum3] Lishuang Gong, Jianguo Zhang, Haifang Liu, Luxiao Sang, and Yuncai Wang. True random number generators using electrical noise. *IEEE Access*, PP:1–1, 09 2019.

[Addendum4] Priyanka, Imran Hussain, and Aqeel Khalique. Random number generators and their applications: A review. 7:1777–1781, 06 2019.

[Addendum5] quantumbase. playing dice with lottery tickets.

[Addendum6] Sinjin Baglin. Random numbers and gaming. 2017.

[Addendum7] Britannica. The editors of encyclopaedia. 'stochastic process', 2023.

[Addendum8] Ben Geller  Joe Redish. Diffusion and random walks, 2011.

[Addendum9] Lingqi Meng and Naoki Masuda. Analysis of node2vec random walks on networks. *Proceedings of the Royal Society A*, 476(2243):20200447, 2020.

[Addendum10] Shayan A. Tabrizi, Azadeh Shakery, Masoud Asadpour, Maziar Abbasi, and Mohammad Ali Tavallaie. Personalized pagerank clustering: A graph clustering algorithm based on random walks. *Physica A: Statistical Mechanics and its Applications*, 392(22):5772–5785, 2013.

[Addendum11] Sooyeong Kim, Jane Breen, Ekaterina Dudkina, Federico Poloni, and Emanuele Crisostomi. On the effectiveness of random walks for modeling epidemics on networks. *Plos one*, 18(1):e0280277, 2023.

[Addendum12] Stephen D. Durham, Nancy Flournoy, and William F. Rosenberger. A random walk rule for phase i clinical trials. *Biometrics*, 53(2):745–760, 1997.

[Addendum13] DWO Rogers. Monte carlo techniques in radiotherapy. *Physics in Canada*, 58(2):63–70, 2002.

[Addendum14] FasterCapital. Monte carlo simulation for portfolio management: an overview and some examples, 2024.

[Addendum15] Powered by AI and the LinkedIn community. How can you use monte carlo methods to analyze weather's impact on operations?, 2024.

[Addendum16] Hamid Gholami, Setareh Rahimi, Aboalhasan Fathabadi, Samaneh Habibi, and Adrian L Collins. Mapping the spatial sources of atmospheric dust using glue and monte carlo simulation. *Science of the total environment*, 723:138090, 2020.

[Addendum17] Philippe Baratta, Julien Bel, Stephane Plaszczynski, and Anne Ealet. High-precision monte carlo modelling of galaxy distribution. *Astronomy & Astrophysics*, 633:A26, 2020.

[Addendum18] HT MacGillivray, RJ Dodd, JF Lightfoot, AS Trew, and BV McNally. Monte-carlo simulation of the orientations of galaxies in clusters. *Astrophysics and Space Science*, 70:385–392, 1980.

[Addendum19] CADENCE PCB SOLUTIONS. The use of the monte carlo method in sensitivity analysis and its advantages, 2023.